“Candidatus Siderophilus nitratireducens”

a putative nap-dependent nitrate-reducing iron oxidizer within the new order Siderophiliales

Corbera Rubio, F.; Stouten, G.R.; Bruins, Jantinus; Dost, Simon F.; Merkel, Alexander Y.; Müller, S.; van Loosdrecht, Mark C.M.; van Halem, D.; Laureni, M.

DOI
10.1093/ismeco/ycae008

Publication date
2024

Document Version
Final published version

Published in
ISME Communications

ISME Communications, 2024, 4(1), ycae008
https://doi.org/10.1093/ismeco/ycae008
Advance access publication: 20 January 2024
Original Article

"*Candidatus* Siderophilus nitratireducens": a putative *nap*-dependent nitrate-reducing iron oxidizer within the new order Siderophiliales

Francesc Corbera-Rubio[1], Gerben R. Stouten[1], Jantinus Bruins[2], Simon F. Dost[3], Alexander Y. Merkel[4], Simon Müller[1], Mark C.M. van Loosdrecht[1], Doris van Halem[1], Michele Laureni[1,*]

[1]Delft University of Technology, Stevinweg 1, 2628 CN Delft, the Netherlands
[2]WLN, Rijksstraatweg 85, 9756 AD Glimmen, the Netherlands
[3]WMD Water Company Drenthe, Lauwers 3, 9405 BL Assen, the Netherlands
[4]Winogradsky Institute of Microbiology, Research Center of Biotechnology, Russian Academy of Sciences, 60 let Oktjabrja pr-t, 7, bld. 2, 117312 Moscow, Russia

*Corresponding author: Michele Laureni, Civil Engineering and Geosciences Faculty, Delft University of Technology, Stevinweg 1, 2628 CN Delft, The Netherlands. Email: m.laureni@tudelft.nl

Abstract

Nitrate leaching from agricultural soils is increasingly found in groundwater, a primary source of drinking water worldwide. This nitrate influx can potentially stimulate the biological oxidation of iron in anoxic groundwater reservoirs. Nitrate-dependent iron-oxidizing (NDFO) bacteria have been extensively studied in laboratory settings, yet their ecophysiology in natural environments remains largely unknown. To this end, we established a pilot-scale filter on nitrate-rich groundwater to elucidate the structure and metabolism of nitrate-reducing iron-oxidizing microbiomes under oligotrophic conditions mimicking natural groundwaters. The enriched community stoichiometrically removed iron and nitrate consistently with the NDFO metabolism. Genome-resolved metagenomics revealed the underlying metabolic network between the dominant iron-dependent denitrifying autotrophs and the less abundant organoheterotrophs. The most abundant genome belonged to a new *Candidate* order, named Siderophiliales. This new species, "*Candidatus* Siderophilus nitratireducens," carries genes central genes to iron oxidation (cytochrome *c cyc2*), carbon fixation (*rbc*), and for the sole periplasmic nitrate reductase (*nap*). Using thermodynamics, we demonstrate that iron oxidation coupled to *nap* based dissimilatory reduction of nitrate to nitrite is energetically favorable under realistic Fe^{3+}/Fe^{2+} and NO_3^-/NO_2^- concentration ratios. Ultimately, by bridging the gap between laboratory investigations and nitrate real-world conditions, this study provides insights into the intricate interplay between nitrate and iron in groundwater ecosystems, and expands our understanding of NDFOs taxonomic diversity and ecological role.

Keywords: NDFO, iron, nitrate, groundwater

Introduction

Globally, approximately one-third of the nitrogen applied to agricultural soils is lost via leaching to the surrounding waterbodies [1]. This has led to elevated nitrate (NO_3^-) levels in anoxic groundwaters, a primary source of drinking water worldwide [2]. Owing to population growth and agriculture intensification, nitrate concentrations in subsurface waters are expected to continue increasing [3]. Besides its direct impact on human health [4], nitrate can significantly alter the biogeochemistry of groundwater reservoirs [5]. Nitrate promotes the oxidation of sulfide and in particular of iron (Fe) – the most prevalent groundwater contaminant – leading to the formation of oxides with high adsorption capacity and the emission of greenhouse gases [6]. Despite these implications, the consequences of nitrate–iron interactions on ecosystems and drinking water production systems remain largely unexplored. A detailed understanding of the underlying principles is paramount for anticipating and mitigating current and future challenges, as well as for exploring potential synergies and biotechnological opportunities.

Nitrate-dependent iron-oxidizing (NDFO) bacteria, also referred to as nitrate-reducing iron-oxidizers (NRFO) [7, 8], couple the anoxic reduction of nitrate to the oxidation of Fe^{2+} (eq. 1). Since their discovery in 1996 by Straub *et al.* [9], NDFO microorganisms have been the focus of extensive research both in pure and mixed cultures (reviewed in [10]), and several complete genomes are already publicly available [11, 12]. The metabolic versatility of NDFO bacteria spans from lithoautotrophic to mixotrophic growth [10], to partial denitrification using nitric oxide (NO) [13] and nitrous oxide (N_2O) [11] as terminal electron acceptors. At the same time, due to the inherently low energetic yield of iron oxidation, NDFO bacteria live close to the thermodynamic edge [14]. Their fitness is highly dependent on environmental factors such as substrate and product availability, pH and temperature [15]. Chemical reactions – such as the quasi-instantaneous

Received: 16 September 2023. **Revised:** 3 January 2024. **Accepted:** 17 January 2024

precipitation of the biologically formed Fe^{3+} – can play a pivotal role by modulating iron and nitrogen concentrations [16]. However, our current understanding is largely based on laboratory settings, and does not necessarily reflect the complexity of natural and engineered ecosystems where several (a)biotic reactions occur simultaneously at temperatures significantly lower than tested to date [17].

$$10Fe^{2+} + 2NO_3^- + 24\,H_2O \rightarrow 10Fe(OH)_3 + N_2 + 18H^+ \quad (1)$$

To address these knowledge gaps, we established a pilot-scale filter on anoxic groundwater containing both Fe^{2+} and NO_3^-. The emulated groundwater conditions allowed for the establishment of a microbial enrichment that simultaneously removed Fe^{2+} and NO_3^-. In depth metagenomic analysis of the steady-state community revealed a new order-level NDFO lineage, deepening our understanding of their taxonomic diversity and ecological roles. Overall, our study bridges the gap between laboratory studies and real-world conditions, and offers a nuanced view on the intricate interplay between nitrate and iron in groundwater ecosystems.

Results

Nitrate-dependent iron removal irrespective of the limiting nutrient

A pilot-scale, granular activated-carbon filter was fed with nitrate-rich anoxic groundwater for 120 days. Stable anoxic nitrate and iron removals were achieved after less than 3 weeks of operation and maintained for over 100 days (Fig. 1). With nitrate as the limiting nutrient at both groundwater (8.9 ± 2.8 μM) and nitrate-amended concentrations (13.5 ± 1.5 and 20.2 ± 2.4 μM), effluent nitrate concentrations were consistently below detection limit (1 μM). Throughout the nitrate-limiting period, NO_3^- and Fe^{2+} were consumed at a 7.1 ± 1.4 Fe^{2+}:NO_3^- molar ratio (Fig. S3). Oxygen was always below the quantification limit of 3 μM. Roughly 80 μC-mol dissolved organic carbon (DOC·l^{-1}) was consistently removed from the influent, likely due to Fe^{2+}–DOC complexes formation owing to the non-biodegradable nature of organic matter in the groundwater matrix (<1.2 μC-mol·l^{-1} assimilable organic matter). Ammonia consumption was negligible (<0.1 μM). Effluent nitrite concentrations stayed below the detection limit (<0.2 μM), while other denitrification intermediates – nitric oxide and nitrous oxide – were not measured. The observed consistent stoichiometric coupling between nitrate and iron removals strongly suggests Fe^{2+} oxidation to be primarily driven by microbial nitrate-reducing iron oxidation.

Microbial community dominated by iron oxidizers and denitrifiers

Metagenomic DNA sequencing yielded a total of 107 512 and 8 754 261 quality filtered short and long reads, respectively. After assembly and polishing, this resulted in 19 127 contigs with an N50 value of 15 927. Contigs binning resulted in 13 high (>90% completeness and <5% contamination; containing full-length 23S, 16S, and 5S ribosomal RNA genes and ≥18 transfer RNA genes) and medium (completeness >50% and contamination <10%) quality metagenome assembled genomes (MAGs) as defined by [18] with a relative abundance exceeding 0.5% of the quality filtered long reads. Collectively, these 13 most abundant genomes accounted for 66.9% of the total quality filtered reads, and belonged to four phyla: *Proteobacteria* (51.6%), *Actinobacteria* (8.3%), *Bacteroidetes* (5.6%), and *Chloroflexi* (1.4%) (Table 1). All genomes

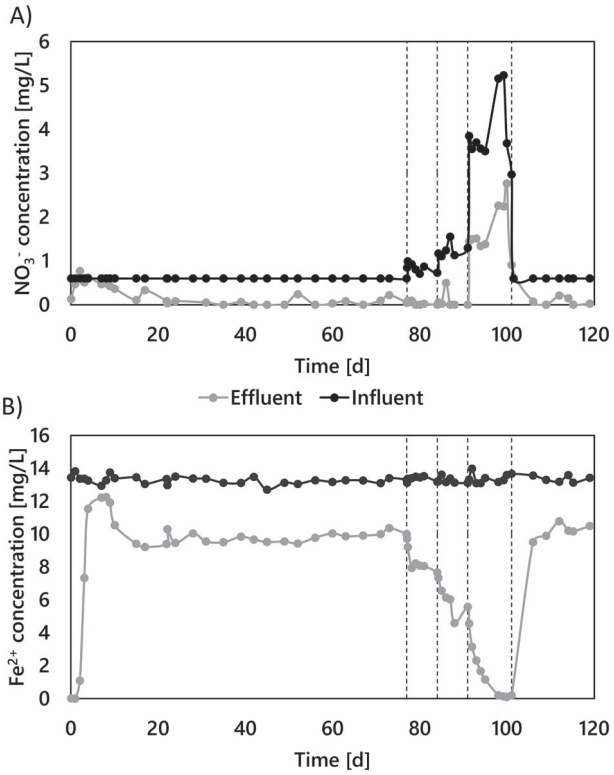

Figure 1. Simultaneous NO_3^- (A) and Fe^{2+}(B) removals in the groundwater-fed pilot-scale filter during the 120 days of continuous operation. The groundwater Fe^{2+} concentration was constant throughout the experiment (236 ± 4 μM). NO_3^- was dosed in the influent to increase the natural groundwater concentration in steps from 8.1 ± 2.1 to 20.2 ± 2.4 μM (NO_3^- limitation), and up to 83.8 ± 0.6 μM (Fe^{2+} limitation). Fe^{2+} and NO_3^- were proportionally removed throughout the whole experiment, regardless of the limiting nutrient (see Fig. SI 3).

in the community contained at least one gene encoding for a denitrifying enzyme, and five featured the genetic potential for iron oxidation. Notably, all putative iron oxidizers also possessed the genetic repertoire for carbon fixation. The most abundant MAG (MAG.13), accounting for 19.3% of the community, could only be taxonomically classified at class level (*Gammaproteobacteria*). Given its high abundance and potential metabolic relevance, the taxonomy and metabolic potential of MAG.13 was further investigated (Table S1).

"*Candidatus* Siderophilus nitratireducens" represents a new order within Gammaproteobacteria

Our phylogenomic analysis based on the concatenated amino acid sequences of 120 bacterial single copy conservative marker genes revealed that MAG.13 (98.6% completeness, 1.7% contamination) belongs to a bacterium forming a new order-level lineage Ga0077554 (GTDB release 08-RS214), within the class *Gammaproteobacteria*, with no known closely related pure-culture representatives (Fig. 2). We propose to name the new species "*Candidatus* Siderophilus nitratireducens" gen.nov., sp.nov., a member of the *Candidate* order and family Siderophiliales and Siderophiliaceae, respectively. This lineage, along with several other MAGs from similar groundwater habitats [21], is mostly related to lineages including lithoautotrophic sulfur-oxidizing bacteria from the genera *Sulfuriflexus*, *Thioalbus*, and the members of the order *Thiohalomonadales*, including *Thiohalomonas*, *Sulfurivermis*, and *Thiohalophilus*. Average nucleotide identity and in-silico calculated

Table 1. General characteristics of the MAGs recovered from the pilot-scale filter. The last three columns indicate the presence/absence of the essential genes for iron oxidation, denitrification, and carbon fixation via the reductive phosphate pentose phosphate cycle. Cov_il and cov_np are the coverage with Illumina short reads and Nanopore long reads, respectively.

MAG ID	Phylogenetic affiliation	Phylum	Relative abundance (%)	Scaffolds	N50	GC (%)	Completeness (%)	Contamination (%)	cov_il	cov_np	Coding genes	MAG quality	Iron oxidation[a]	Denitrification[b]	Carbon fixation[c]
MAG.13	**"*Candidatus* Siderophilus nitratireducens"	Proteobacteria	19.3	9	18,97 007	56	98.59	1.73	298.27	300.86	3217	High	Yes	NO_3^+ – > NO_2^-	Yes
MAG.26	f__Gallionellaceae	Proteobacteria	10.0	10	5,69 264	55	95.81	0.95	234.92	155.81	3749	High	Yes	NO_3^+ – > NO; N_2O - > N_2	Yes
MAG.18	f__Anaeromyxobacteraceae	Proteobacteria	8.6	21	5,18 414	73	98.06	0.65	186.12	131.88	4018	High	No	N_2O - > N_2	No
MAG.19	g__*Devosia*	Proteobacteria	6.5	27	41,38 465	64	99.28	0.14	24.53	100.33	4029	High	No	NO_2^- - > NO	No
MAG.10	f__Chitinophagaceae	Bacteroidetes	5.6	4	36,46 631	40	97.54	0.9	304.83	87.01	3193	High	No	NO - > N_2	No
MAG.03	o__Nanopelagicales	Actinobactiria	4.3	11	7,79 605	69	99	2.37	140.41	67.49	4065	High	No	NO_3^- - > NO	No
MAG.27	o__Nanopelagicales	Actinobactiria	3.9	9	11,66 278	71	98.3	1.98	140.56	60.77	3910	High	No	NO_3^- - > NO	No
MAG.34	g__*Gallionella*	Proteobacteria	3.5	112	46 607	57	95.91	3.25	64.39	52.65	2516	High	Yes	NO_3^- - > NO	Yes
MAG.00	o__Anaerolineales	Chloroflexi	1.4	100	1,14 338	55	97.27	2.91	21.93	20.04	4828	High	No	NO_2^- - > NO	No
MAG.08	g__*Rhodoferax*	Proteobacteria	1.2	121	69 171	63	88.95	2.37	33.64	17.42	3870	Medium	No	NO_3^- - > NO	Yes
MAG.04	f__Rhizobiaceae	Proteobacteria	0.9	115	80 809	60	95.12	4.1	25.97	13.93	4768	High	No	NO_3^- - > N_2O	No
MAG.16	f__Gallionellaceae	Proteobacteria	0.9	165	27 226	56	88.51	3.94	52.76	13.55	3002	Medium	Yes	NO_3^- - > N_2O	Yes
MAG.29	g__*Rhizobacter*	Proteobacteria	0.7	257	25 511	66	94.54	4.54	21.73	9.94	4225	Medium	Yes	NO_3^+ – > NO_2^-	Yes

[a]Based on FeGenie [19]. "Yes" if either cyc2, cyc1, foxABC, foxEYZ, sulfocyanin, pioABC, or mtoAB are present. [b]Based on GhostKOALA [20] and the presence of napAB or narGHI (K02567, K02568, or K00370, K00371, K00374; $NO_3^- \rightarrow NO_2^-$), nirK or nirS (K00368, K15864; $NO_2^- \rightarrow NO$), norBC (K04561, K02305; $NO \rightarrow N_2O$), nosZ (K00376; $N_2O \rightarrow N_2$) from denitrification (M00529). [c]Based on GhostKOALA [20]. "Yes" if either rbcL (K01601) or rbcS (K01602) and prkB (K00855) from reductive phosphate pentose phosphate cycle (Calvin Cycle) (M00165). **Initially classified as c_Gammaproteobacteria.

DNA–DNA hybridization comparison between "*Ca.* Siderophilus nitratireducens" and its closest relative, a MAG from a drinking water treatment plant (GCA_001464965.1), indicated that the two organisms belong to the same genus but different species (ANI = 89%, DDH = 36.6%).

Autotrophy in "*Ca.* Siderophilus nitratireducens"

To resolve the main anabolic and catabolic pathways of "*Ca.* Siderophilus nitratireducens," open reading frames (ORFs) were predicted and annotated (Table 2, detailed version in Table S1). The genome contains marker genes coding for two key proteins of autotrophic CO_2 fixation via the reductive pentose phosphate (Calvin–Benson–Bassham; CBB) cycle, including the large and small subunits of the ribulose-1,5-bisphosphate carboxylase-oxygenase (*rbc*LS form I) and the phosphoribulokinase (*prk*). Genes encoding for carboxysomal shell proteins and carbonic anhydrase were also present, further supporting the inorganic carbon uptake ability of "*Ca.* Siderophilus nitratireducens". The absence of phosphofructokinase (*pfk*) indicates a modified glycolytic pathway initiating at the glyceraldehyde 3-phosphate level. All tricarboxylic acid (TCA) cycle genes were identified except for fumarate hydratase (*fh*). However, the glyoxylate shunt enzymes malate synthase (*glc*B) and isocitrate lyase (*ace*A) were present. Taken together, these findings suggest the capability for full autotrophic growth of "*Ca.* Siderophilus nitratireducens."

Iron oxidation in "*Ca.* Siderophilus nitratireducens"

The presence of a monoheme *c* cytochrome *cyc*2 cluster 3, a primary iron oxidation gene, suggests that "*Ca.* Siderophilus nitratireducens" can use Fe^{2+} as an electron donor. Other common Fe^{2+} oxidases, namely the diheme *c* cytochrome cyc1 and the multiheme c cytochromes MtoA and MtoB, were not annotated. Despite the close phylogenetic proximity to lithoautotrophic sulfur-oxidizing bacteria, the genes of sulfide dehydrogenases Sqr and FccAB and sulfite dehydrogenases SorAB and SoeABC were not identified.

In terms of potential catabolic electron acceptors, the genes for a periplasmic nitrate reductase (*nap*ABCD and its membrane ferrodoxins *nap*GH) and a cbb_3-type cytochrome c oxidase (*cco*NOP) were annotated. However, genes encoding for other known denitrification reductases, namely membrane-bound nitrate reductase (*nar*GHI) and nitrite, nitric oxide and nitrous oxide reductases, *nir*K/*nir*S, *nor*BC, and *nos*Z respectively, were not found (Table 2, detailed version in Table S1). Additionally, alternative oxidases, such as the cytochrome *bd* ubiquinol oxidase (*cyd*AB) or the aa_3-type cytochrome c oxidase (*cox*ABCD) were not identified. Also, genes of dissimilatory sulfate reduction (*apr*AB and *dsr*ABC) and the *sox* complex, responsible for sulfate reduction could not be identified. These findings suggest that "*Ca.* Siderophilus nitratireducens" relies exclusively on nitrate and oxygen as electron acceptors.

On the thermodynamic feasibility of nap-dependent nitrate-reducing iron-oxidation

Based on its genome, "*Ca.* Siderophilus nitratireducens" is potentially an autotrophic organism that obtains energy by oxidizing Fe^{2+} to Fe^{3+} while reducing NO_3^- to NO_2^-. Yet, as iron is a weak electron donor, the standard Gibbs free energy of the reaction is positive under standard biological conditions (pH 7). The process

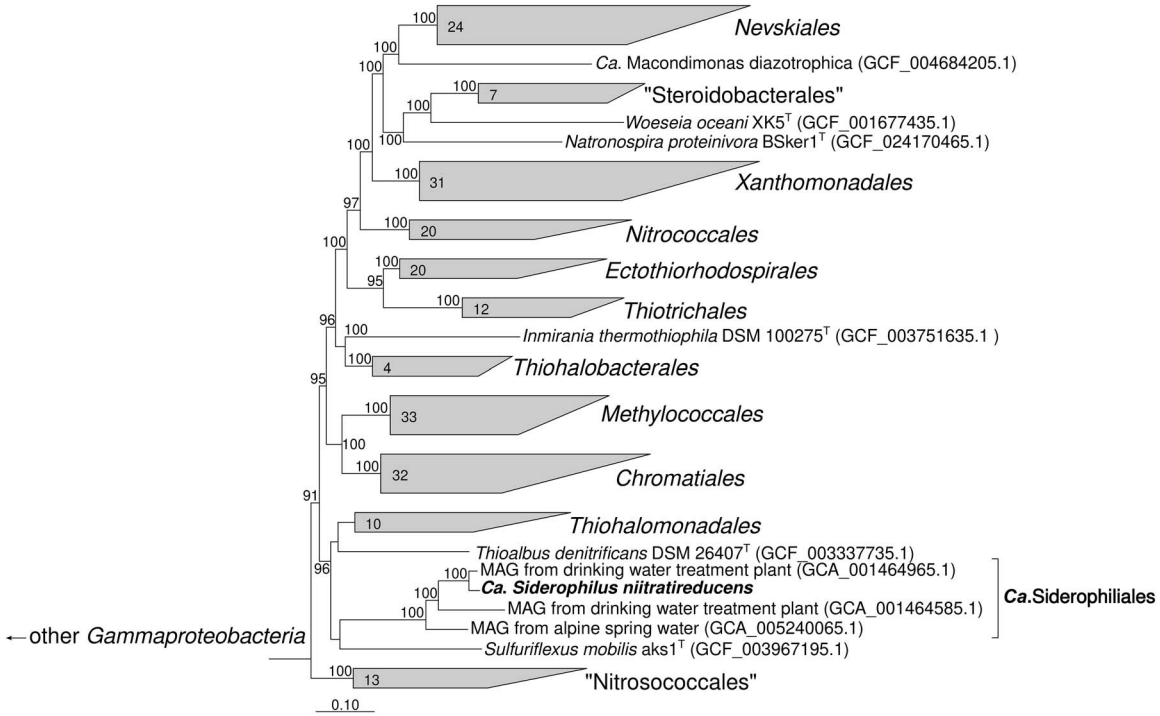

Figure 2. Phylogenetic position of the "*Ca.* Siderophilus nitratireducens" based on sequence analyses of concatenated alignment of 120 single-copy conserved bacterial protein markers [22] – taxonomic designations correspond to the Genome Taxonomy DataBase 207). The trees were built using IQ-TREE2 [23] with approximate likelihood-ratio test for branches [24]. Bootstrap consensus tree is shown with values above 90% placed at the nodes. Bar, 0.10 changes per position.

Table 2. Key enzyme of the main catabolic and anabolic pathways of "Ca. Siderophilus nitratireducens." "+" and "–"indicate presence or absence in the genome. CBB, Calvin–Benson–Bassham cycle; TCA, Tricarboxylic acid cycle/Krebs cycle.

Electron acceptor			Electron donor			Carbon fixation			Carbon metabolism		
Element	**Key genes**	**Presence**	**Element**	**Key genes**	**Presence**	**Pathway**	**Key genes**	**Presence**	**Pathway**	**Key genes**	**Presence**
Nitrogen	*nap*ABCD	+	Iron	*cyc2*	+	CBB	*rbc*LS form I	+	Glycolysis	*pfk*	–
	*nar*GHI	–		*cyc1*	–		*prk*	+		*gpml*	+
	*nir*KS/*nor*BC/*nos*Z	–		*mto*AB	–		Carboxysome	+	TCA cycle	*cs / glt*A	+
Sulfur	*apr*AB	–	Sulfur	*sqr*	(+)					*suc*AB	+
	*sox*XABYZ(CD)	–		*fcc*AB	–					*fh*	–
Oxygen	*cco*NOP	+								*mdh*	+
	*qox*ABCD	–							Glyoxylate	*glc*B	+
	*cyd*ABX	–							shunt	*ace*A	+

is therefore thermodynamically unfavorable:

$$Fe^{2+} + 0.5NO_3^- + H^+ \rightarrow Fe^{3+} + 0.5NO_2^- + 0.5H_2O \; \Delta G^{01} = 35.2 \frac{kJ}{e\text{–}mol}$$

However, the exceptionally low solubility constants of iron oxides, ranging from 10^{-34} to 10^{-42} [25] result in very low Fe^{3+} concentrations. Thereby, precipitation creates the conditions for a favorable thermodynamic driving force for the oxidation of Fe^{2+} to Fe^{3+} [26]. Under the operational conditions of this study (283 K, <1 $\mu molNO_3^- \cdot l^{-1}$, <0.2 $\mu molNO_2^- \cdot l^{-1}$ in the effluent), the reaction becomes thermodynamically favorable owing to the calculated Fe^{3+}/Fe^{2+} ratio in the order of 10^{-16} (conservative value, see Section 4.2):

$$\Delta G^1 = \Delta G_r^{01} + RTln\left[\frac{[Fe^{3+}][NO_2^-]^{\frac{1}{2}}}{[Fe^{2+}][NO_3^-]^{\frac{1}{2}}}\right] = -66.2 \frac{kJ}{e\text{–}mol}$$

A Gibbs free energy of −66 kJ/e-mol is in principle enough to transport three to four protons over the cytoplasmic membrane, considering a value of 15 $kJ \cdot mol_{H+}^{-1}$ [27], and would yield at least one ATP. If other iron precipitation products are formed, the redox potential of Fe^{2+}/Fe^{3+} increases further. Even at more conservative Fe^{3+}/Fe^{2+} ratios and pH, due to non-equilibrium conditions and product gradients, the biological process remains favorable (Fig. 3).

Complete denitrification: a collaborative effort of iron-oxidizing autotrophs and organoheterotrophs

Iron oxidation genes were identified in five MAGs, namely MAG.13 ("*Ca.* Siderophilus nitratireducens"), MAG.29 (g_*Rhizobacter*) and MAG.26, MAG.34 and MAG.16 (f_*Gallionellaceae,* commonly associated with autotrophic iron oxidation). These MAGs also encoded for the central enzymes of the carbon dioxide fixation

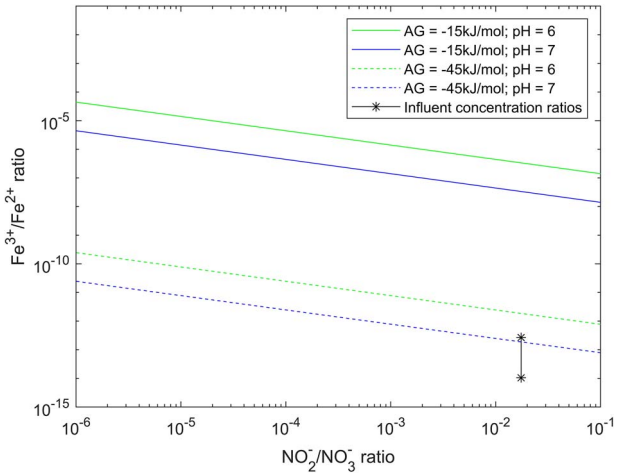

Figure 3. Gibbs energy dissipated during nitrate-reducing iron oxidation as function of the ratio of substrates and products. As reference, lines represent the ratios at which the minimum energy required to generate pmf (−15 kJ·Mol^{-1}, full lines) and ATP (−45 kJ·Mol^{-1}, dashed lines) is generated at intracellular pH of 6 (green) or 7 (blue) ([27]). Star dots represent the actual ratios based on measured ($NO_2^-/NO_3^-/Fe^{2+}$) and calculated (Fe^{3+}) influent reactor concentrations. Note that NO_2^- was below detection limit (< 0.2 μmol·l^{-1}), so that the actual reactor conditions were likely even more favorable, i.e. more on the left .

via the CBB cycle. While all 13 MAGs contained genes encoding for at least one denitrification enzyme (Table 2), none of them possessed a comprehensive gene set to fully reduce nitrate to dinitrogen gas. Dissimilatory nitrate reduction to nitrite, the first denitrification step, was present in nine MAGs, while the final step, nitrous oxide reduction to nitrogen gas, was only found in MAG.26 (g_*Rhizobacter*), MAG.18 (f_*Anaeromyxobacteraceae*) and MAG.10 (f_*Chitinophagaceae*). The five most abundant MAGs (>5%) alone accounted for up to 50% of the community and covered the full denitrification (Fig. 4). All putative iron oxidizers also possessed the genetic potential for aerobic respiration (i.e. they contained *cbb*$_3$-type terminal oxidases). Interestingly, two distinct potential niches were identified. The autotrophic iron oxidizers, "*Ca*. Siderophilus nitratireducens" and MAG.26 (f_*Gallionelleceae*), performed the initial denitrification reductions, while the lower-abundant organoheterotrophs complemented the reduction of (at least) NO to nitrous oxide possibly taking advantage of the autotrophically fixed carbon excreted by the iron oxidizers. Due to the absence of sufficient biodegradable organic matter in the influent, a portion of the biologically generated NO was likely reduced to N_2O chemically with Fe^{2+} [28].

Discussion

We established a pilot-scale filter on nitrate-rich anoxic groundwater to elucidate the structure and metabolism of nitrate-reducing iron-oxidizing microbial communities under oligotrophic conditions mimicking natural groundwater. The enriched microbial community stoichiometrically removed iron and nitrate during more than 4 months, and was dominated by a genome belonging to a new *Candidate* order, named Siderophiliales. The genome of this new species, "*Ca*. Siderophilus nitratireducens," encoded the genes for iron oxidation (cytochrome *c cyc2*) and, within the denitrification pathway, the periplasmic nitrate reductase (*nap*). The absence of other denitrification genes suggests a short catabolic path, which may offer a kinetic advantage in terms of higher iron oxidation rates [29] especially under nitrogen limiting conditions [30]. In contrast, the majority of NDFO genomes reported so far encode the membrane-bound nitrate reductase (*nar*) along with other downstream denitrification genes [11, 31-34]. *Nar* actively translocates protons, whereas *nap* conserves energy only indirectly by accepting electrons from the quinol pool on the periplasmic side of the membrane, effectively consuming cytoplasmic protons [35]. Recently, novel Zetaproteobacteria genomes possessing *nap* have been recovered from a complex community, yet they also possessed at least another energy conserving nitrogen oxide [5, 36]. The presence of a *cbb*$_3$-type cytochrome *c* oxidase suggests that "*Ca*. Siderophilus nitratireducens" may also be capable of oxygen respiration. This is consistent with the fact that all reported genomes of anaerobic iron-oxidizing bacteria contain oxygen reductases [31, 34, 37], including the well-studied KS [13] and AG [38] cultures. However, to the best of our knowledge, NDFO growth under (micro)aerophilic conditions has not been reported to date [11]. Although the sporadic detection of traces of oxygen (<3 μM) in our filter does not allow to fully exclude aerobic activity, and in the absence of cultured representatives to confirm it, we posit that *nap*-driven iron oxidation was the primary catabolic route of "*Ca*. Siderophilus nitratireducens" under the *in-situ* restricted availability of alternative substrates. Furthermore, "*Ca*. Siderophilus nitratireducens" was also identified as a putative autotroph, adding the additional challenge of energy and electrons needs for anabolic CO_2 fixation to the growth on iron, a weak electron-donor at standard conditions [15]. Thermodynamic evaluations indicate that *nap*-dependent iron oxidation can sustain growth at realistic Fe^{3+}/Fe^{2+} and NO_3^-/NO_2^- concentrations ratios. To this end, the quasi-instantaneous precipitation of the biologically formed Fe^{3+} as iron oxides under circum-neutral pH plays a central role as thermodynamic driving force [39]. The specific mechanisms by which this thermodynamic potential is harnessed for carbon fixation remain to be fully elucidated.

The subsequent reduction of the produced nitrite resulted from the concerted activity of putative autotrophic iron-oxidizers and organoheterotrophs. Within the microbial community, the second most abundant genome, MAG.26 (f_*Gallionellaceaea*), featured the genetic potential for iron oxidation and most denitrification steps, with the exception of nitrous oxide reductase (*nor*). MAG.26 also possessed the cytochrome *c* oxidase *cbb*$_3$-type *cco*NOP for aerobic respiration. Interestingly, this genome contained genes for CO_2 fixation, a trait mirrored in all other less abundant genomes with the ability to oxidize iron. This suggests that autotrophy may represent an essential trait for NDFOs in anoxic groundwaters where the dissolved organic carbon is largely non-biodegradable [40]. The three second most abundant genomes, MAG.18 (f_*Anaeromyxobacteraceae*), MAG.19 (g_*Devosia*) and MAG.10 (f_*Chitinophagaceae*) were found to lack the genes for iron oxidation and CO_2 assimilation. Yet, these genomes encompassed the full denitrification pathway starting from nitrite. Besides the likely occurrence of chemical reduction of NO to N_2O [41], we speculate that these heterotrophs complemented the NDFOs for at least the reduction of NO using autotrophically fixed organic carbon as substrate. A similar metabolic network was also recently observed in mesophilic NDFO communities [13]. Overall, the measured iron and nitrate consumption yield of 7.1 mol Fe^{2+}: mol NO_3^- is consistent with the expected 5.6, i.e. considering the theoretical catabolism (eq. 1) and the recently estimated 12% of electrons used for growth [7], but higher than the experimentally observed range of 3.8–4.7 [9, 31, 42]. At first, we hypothesized nitrate ammonification to be the reason for

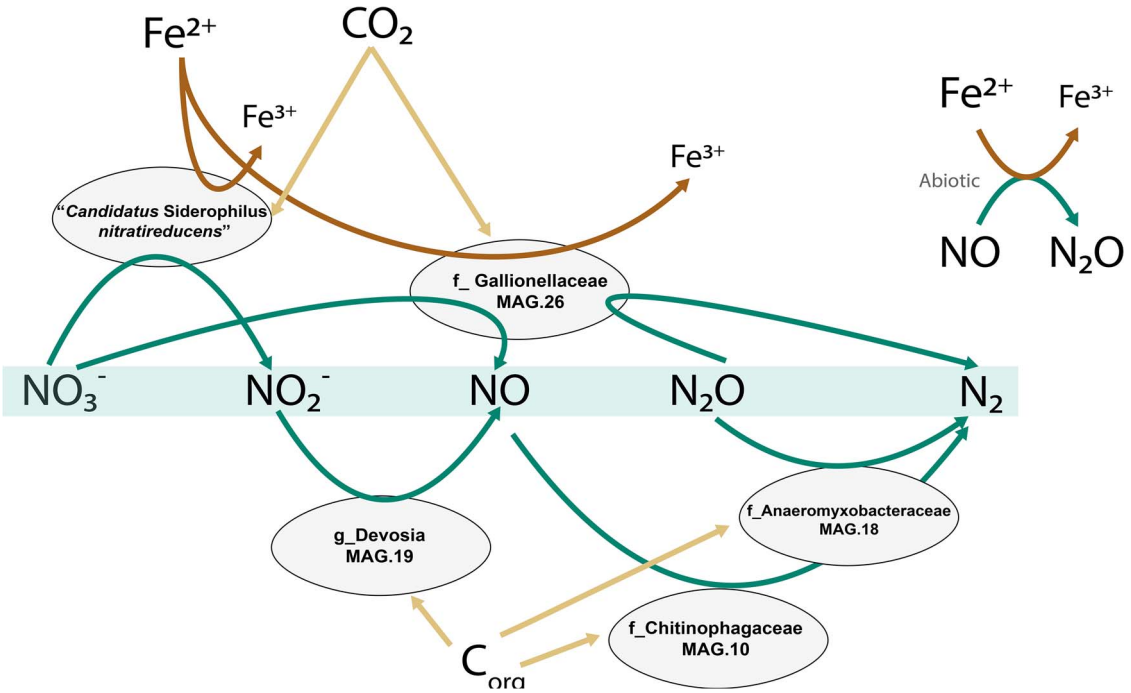

Figure 4. Genome-based conceptual model of substrates fluxes within the microbial community represented by the five most abundant MAGs. Putative autotrophic iron oxidizers perform the upstream part of denitrification, while flanking communities reduce the toxic intermediates to innocuous dinitrogen gas. The putative autotrophic metabolism was inferred based on the presence of ribulose-1,5-biphosphate carboxylase/oxygenase (RuBisCO) and phosphofructokinase (pfk).

the slight excess in iron oxidation, yet none of the putative iron-oxidizing genomes encoded for the common *nrf* nor for the newly reported octaheme complex [43]. Also, the oxygen sporadically detected in the influent was always below the quantification limit of 3 μM, a conservative concentration that alone would explain less than 15% of the total iron consumption via chemical oxidation. As no Fe^{3+} was detected in the reactor effluent, all iron necessarily accumulated inside the reactor either as Fe^{2+} or Fe^{3+} precipitates. X-ray diffraction and Mössbauer spectroscopy identified over 94% of the Fe in solids as amorphous ferrihydrite, an Fe^{3+} oxide, with <6% of the solids attributed to magnetite, an Fe^{2+}–Fe^{3+} oxide typically formed under anaerobic conditions (Figure S4, Table S2 and SI 5). Consequently, the Fe^{2+} unaccounted for was likely continuously adsorbed onto the newly-formed Fe^{3+} oxides, a well-studied phenomenon [44], yet the extent to which this occurred was not investigated. In conclusion, pending experimental validation, we surmise that NDFO microorganisms may not only contribute to iron removal by direct oxidation but also by continuously providing newly-formed iron oxides for its adsorption.

Description of "*Ca.* Siderophilus nitratireducens" gen. nov., sp. nov.

Siderophilus (Si.de.ro'phi.lus Gr. masc.n. *sidêros* iron; Gr. masc. adj. *philos* loving; N.L. masc. n. *Siderophilus*, loving iron).

ni.tra.ti.re.du'.cens (N.L. masc. n. *nitras (gen. nitratis)*, nitrate; L. pres. part. *reducens*, converting to a different state; N.L. part. adj. *nitratireducens*, reducing nitrate).

Autotrophic nitrate-reducing iron-oxidizing bacterium isolated from a filtration unit fed with anaerobic groundwater with iron(II) and nitrate. Harbors also have the genetic potential to aerobically oxidize iron.

Materials and methods

Groundwater and pilot-scale filter characteristics

An iron reducing microbial community was enriched anoxically on the granular activated carbon of a 10-L pilot-scale filter in Emmen (the Netherlands) (Figs S1 and S2 and Table S1). The media was devoid of any previously formed biofilm. The anoxic, nitrate-rich groundwater (−75.2 ± 28.4 mV) featured constant Fe^{2+} and NO_3^- concentrations, 236 ± 4 μM and 8.1 ± 2.1 μM, respectively (Table 3). Oxygen was consistently below quantification limit (3 μM). The groundwater pH and temperature were 6.7 ± 0.2 and 10.5 ± 0.1°C, respectively. The filter was operated at a filtration flowrate of 3.8 m·h^{-1} (29.6 L·h^{-1}) during 120 days. After 75 days of steady-state operation, the influent nitrate concentration was manually increased in four steps up to 83.8 ± 0.6 μM, when the system changed from nitrate ($NO_3^- < 1$ μM) to iron limiting conditions ($Fe^{2+} < 4$ μM).

Dissolved Fe^{3+} estimation

At pH 7, Fe^{3+} has a markedly low solubility and precipitates as iron oxyhydroxide ($Fe(OH)_3$). Thermodynamically, this phase transition favors the oxidation of Fe^{2+} to Fe^{3+}, and the resulting low Fe^{3+} concentration is the primary driving force of equation 1 [45]. In our filter, the dissolved concentration of the Fe^{3+}, resulting from Fe^{2+} oxidation, was always below detection limit (0.01 mg·l^{-1}). To discuss the thermodynamic feasibility of the NDFO process, we estimated the steady-state $[Fe^{3+}]/[Fe^{2+}]$ ratio following the method proposed by Gorski *et al.* [39], which assumes thermodynamic equilibrium between $[Fe^{2+}]$ – $[Fe^{3+}]$ – [FeOx] phases based on the fact that the hydroxylation of dissolved Fe^{3+} is quasi-instantaneous at pH > 3 [46]. Consequently, the following equation can be used to determine the Fe^{3+} concentration as function

Table 3. Influent and effluent water characteristics corresponding to average and standard deviation of daily measurements of Days 21–77, during the nitrate-limited steady-state. Fe^{3+} was calculated as described in the following section.

Parameter	Units	Value	Value
		Influent	Effluent
pH		6.9 ± 0.4	6.7 ± 0.1
T	°C	10.5 ± 0.1	10.9 ± 0.6
ORP	mV	−64 ± 17	−58 ± 18
O_2	$\mu mol \cdot L^{-1}$	<3[a]	<3[a]
NH_4^+	$\mu mol \cdot L^{-1}$	11 ± 1.0	11 ± 8.1
NO_2^-	$\mu mol \cdot L^{-1}$	<0.2[a]	<0.2[a]
NO_3^-	$\mu mol \cdot L^{-1}$	8.1 ± 2.1	<1
Fe^{2+}	$\mu mol \cdot L^{-1}$	236 ± 4	178 ± 5
Fe^{3+}	$\mu mol \cdot L^{-1}$	$2 \cdot 10^{-12}$	
DOC	$mg \cdot L^{-1}$	3.1 ± 0.1	2.0 ± 0.2

[a]Below detection limit

of pH and the solid solubility constant.

$$\left\{Fe^{3+}_{(aq)}\right\}\left\{OH^-\right\}^3 = K_{sp}$$

The most abundant iron oxide in the sand filter was amorphous ferrihydrite (SI 4 and 5), with a K_{sp} of 10^{-39} [46]. Therefore:

$$\left\{Fe^{3+}_{aq}\right\} = \frac{10^{-39}}{\left(10^{-7.1}\right)^3} = 2 \cdot 10^{-18}\ M$$

Analytic procedures

Samples for ammonium, nitrite, and nitrate quantification were immediately filtered through a 0.2 μm nanopore filter and measured within 12 h using photometric analysis (Gallery Discrete Analyzer, Thermo Fischer Scientific, Waltham,MA, USA). Samples for dissolved iron were filtered through a 0.2 μm nanopore filter, acidified to pH < 2 with H_2SO_4, and quantified by ICP-MS (Analytik Jena, Jena, Germany). Temperature, pH, oxidation–reduction potential (ORP), and dissolved oxygen concentration (DO) were monitored daily using a HI9829-01042 multiparameter analyzer (Hanna Instruments, Smithfield, RI, USA) in the raw water, after nitrate dosage and in the effluent.

Biomass sampling, DNA extraction and quality control

Immediately after the end of the experiment, the filter was emptied and the medium grains were completely mixed. A small volume of grains was used for DNA extraction. Nucleic acid extraction was carried out using DNeasy PowerSoil Pro Kit (QIAGEN, Hilden, Germany) following manufacturer instructions. To improve DNA recovery and avoid the interference of carbon with the extraction, 25 μL of 20 $g \cdot l^{-1}$ autoclaved (20 min, 121°C, 2 bar) skimmed milk solution (Sigma Aldrich, Saint Louis, MO, USA) were added to the extraction tube. After extraction, DNA was concentrated to 7.68 ng DNA·μl^{-1} using Microcon centrifugal filter units YM-100 (MilliporeSigma, Burlington, MA, USA) following the manufacturer's instructions. DNA was quantified with the Qubit 4 Fluorometer and Qubit dsDNA HS assay kit (Invitrogen, Waltham, MA, USA) following the manufacturer's instructions. DNA purity was determined using a NanoDrop One Spectrophotometer (Thermo Fisher Scientific, Waltham, MA, USA).

Library preparation, sequencing, and reads processing

Long-read and short-read DNA sequencing were carried out independently. Long-read library preparation was carried out using the ligation sequencing kit SQK-LSK 109 (Oxford Nanopore Technologies, Oxford, UK). R.9.4.1 flowcells on a GridION were used for sequencing. Raw data were basecalled in super-accurate mode using Guppy v.5.0.16 (https://nanoporetech.com). Raw reads were quality-filtered and trimmed using Filtlong (https://github.com/rrwick/Filtlong) to remove reads below 4000 kb and mean quality score below 80. Adapters were removed using Porechop v.0.2.3 (https://github.com/rrwick/Porechop).

Short-read library preparation was performed using the Nextera XT kit (Illumina, San Diego, CA, USA) according to the manufacturer's instructions. The libraries were pooled, denatured, and sequenced with Illumina MiSeq (San Diego, CA, USA). Paired end sequencing of 2 x 300 base pairs was performed using the MiSeq Reagent Kit v3 (San Diego, CA, USA) according to the manufacturer's instructions. Raw sequencing data were quality-filtered and trimmed using Trimmomatic v0.39 (HEADCROP:16 LEADING:3 TRAILING:5 SLIDINGWINDOW:4:10 CROP:240 MINLEN:35) [47]. Sequencing data quality was analyzed using FastQC v0.11.7 before and after trimming [48].

Reads assembly and binning

Reads assembly and binning were done as in [49] with minor modifications. Long-reads were assembled using Flye v. 2.9-b1768 [50] with the "–meta" setting enabled and the "–nano-hq" option. Polishing was carried out with Minimap2 v.2.17 [51], Racon v. 1.3.3 [52], Medaka v.1.4.4 (two rounds) (https://github.com/nanoporetech/medaka). At the end, short-reads were incorporated in a final round of polishing with Racon. Both long- and short-raw reads were independently mapped back to the assembled contigs using BWA-MEM2 [53]. SAMtools v1.14 was used to determine contig coverage and for indexing with default settings [54] .

Automated binning was carried out with the long-reads assembly (polished with short-reads) using MetaBAT2 v. 2.12.1 [55] with "-s 500000," MaxBin2 v. 2.2.7 [56], and Vamb v. 3.0.2 [57] with "-o C–minfasta 500000." Additionally, contig coverage from the short-reads assembly was provided as input to the three binners to improve binning. Output integration and refinement was done in DAS Tool v. 1.1.2 [58] . CoverM v. 0.6.1 (https://github.com/wwood/CoverM) was applied to calculate the bin coverage (using the "-m mean" setting) and the relative abundance ("-m relative_abundance"). Additional manual bin polishing was done in R using mmgenome (https://github.com/MadsAlbertsen/mmgenome).

Assembly processing and gene annotation

The completeness and contamination of the genome bins were estimated using CheckM v. 1.1.2 [59]. The bins were classified using GDTB-Tk v. 1.5.0 [60] 202 database. Barrnap v 0.9 (https://github.com/tseemann/barrnap) and structRNAfinder [61] were used to predict 23S, 16S, and 5S ribosomal RNA sequences, and transfer RNA sequences were determined using tRNAscan-SE v.20 [62] with *default* search mode. Bins were classified using the Minimum Information about a Metagenome-Assembled Genome (MIMAG) standards [18]: high-quality bins were >90% complete and <5% contaminated, and contained full-length 23S, 16S, and 5S ribosomal RNA genes and ≥18 transfer RNA genes. Bins with completeness >50% and contamination <10% were classified as

medium-quality, and bins with completeness <50% and <10% contamination as low-quality bins. The remaining ones were considered contamination. 68% of the filtered reads rendered high- and medium-quality bins, 11% low-quality bins and 21.1% were unbinned.

The ORFs of the 10 resulting high-quality and 3 medium-quality bins with relative abundance >0.5% were predicted using Prodigal v2.6.3 [63] and functionally annotated with GhostKoala v2.2 [20] (Kyota Encyclopedia of Genes and Genomes; accessed March 2022). FeGenie [19] was used to improve the annotation of the iron metabolism using the metagenomics ("-meta") settings. To refine the annotation for MAG.13 (*Candidatus* Siderophilus nitratireducens), the genome was uploaded to the National Center for Biotechnology Information (NCBI) database Prokaryotic Genome Annotation Pipeline v6.1 [64]. Additionally, manual annotation of genes potentially relevant but not automatically annotated was done by aligning a set of manually selected sequences from UniProtKB against the translated ORFs from MAG.13 with local blastp v2.13 [65]. After annotation, all the predicted genes of interest (manually and automatically annotated) were translated and aligned against the Non-redundant protein sequences (nr) database from NCBI using blastp (accessed June 2022) and accepted only if the coverage was >70% [19] and the identity >35% [66].

RStudio v1.4.1106 was used for data analysis and visualization.

Phylogenetic tree construction

Genome-based phylogenetic reconstruction was done by using 120 bacterial single copy conservative marker genes, as described previously [60]. The trees were built using the IQ-TREE 2 [23] with fast model selection via ModelFinder [67] and ultrafast approximation for phylogenetic bootstrap [68], as well as approximate likelihood-ratio test for branches [24]. Whole genome comparison was conducted by using two different methods: Average Nucleotide Identity (ANI), using JSpeciesWS web server and DNA–DNA Hybridization (DDH) by the Genome-to-Genome Distance Calculator 2.1 online tool (https://ggdc.dsmz.de/ggdc.php) [69].

Acknowledgements

The authors would like to thank Dimitry Sorokin (TU Delft and Russian Academy of Sciences) for the thorough discussions and invaluable insights; Martin Pabst and Dita Heikens (TU Delft) for the yet-unpublished proteomic data; Mantas Sereika, Thomas Nielsen, and Mads Albertsen (Aalborg University) for their help with Nanopore Sequencing and genome assembly and binning during the hands-on Nanopore course; Arjan I. Dugulan (Reactor Institute Delft) for the Mossbauer Analysis; and the anonymous Reviewer #2 for the insightful and constructive comments that significantly improved the manuscript.

Author contributions

Francesc Corbera-Rubio, Jantinus Bruins, Mark C. M. van Loosdrecht, Doris van Halem, and Michele Laureni (conceived the study), Jantinus Bruins and Simon F. Dost (designed the filter and performed the on-site experiments), Francesc Corbera-Rubio (run the metagenomics analysis), and Alexander Y. Merkel (the phylogenetic classification). Francesc Corbera-Rubio and Gerben R. Stouten conducted the thermodynamics calculations. Simon Müller performed the solid characterization. Francesc Corbera-Rubio, Gerben R. Stouten, Mark C. M. van Loosdrecht, Doris van Halem, and Michele Laureni performed data analysis and/or helped interpret the results. Francesc Corbera-Rubio wrote the manuscript, with contributions from Gerben R. Stouten, Mark C. M. van Loosdrecht, Doris van Halem, and Michele Laureni. All co-authors critically reviewed the manuscript and approved the final version.

Supplementary material

Supplementary material is available at *ISME Communications* online.

Conflicts of interest

None declared.

Funding

This work was financed by the NWO partnership program "Dunea–Vitens: Sand Filtration" (project 17830) of the Dutch Research Council (NWO) and the drinking water companies Vitens NV and Dunea Duin & Water. M.L. was supported by NWO (VI.Veni.192.252).

Data availability

Raw reads and MAGs have been deposited in the National Center for Biotechnology Information (NCBI) website (https://www.ncbi.nlm.nih.gov/bioproject/) under BioProject PRJNA834785. The BioSample accession numbers for the raw reads and the five most abundant MAGs are SAMN28600298, SAMN28058410 ("*Ca.* Siderophilus nitratireducens"), SAMN36381704 (*f_Gallionelaceae*), SAMN36381891 (*f_Anaeromyxobacteraceae*), SAMN36382736(*g_Devosia*), SAMN36401011 (*f_Chitinophagaceae*).

References

1. Matassa S, Batstone DJ, Hülsen T *et al.* Can direct conversion of used nitrogen to new feed and protein help feed the world? *Environ Sci Technol* 2015;**49**:5247–54. https://doi.org/10.1021/es505432w.
2. Giordano M. Global groundwater? Issues and solutions. *Annu Rev Environ Resour* 2009;**34**:153–78. Available from: https://www.annualreviews.org/doi/abs/10.1146/annurev.environ.030308.100251.
3. Ward MH, Jones RR, Brender JD *et al.* Drinking water nitrate and human health: an updated review. *Int J Environ Res Public Health* 2018;**15**:1557–88. https://doi.org/10.3390/ijerph15071557.
4. WHO. *Guidelines for Drinking-Water Quality, 4th ed. Resuscitation*. Geneva: World Health Organisation, 2010, 26–8.
5. McAllister SM, Vandzura R, Keffer JL *et al.* Aerobic and anaerobic iron oxidizers together drive denitrification and carbon cycling at marine iron-rich hydrothermal vents. *ISME J* 2021;**15**:1271–86. Available from: https://doi.org/10.1038/s41396-020-00849-y. https://www-nature-com.tudelft.idm.oclc.org/articles/s41396-020-00849-y.
6. Schaedler F, Lockwood C, Lueder U *et al.* Microbially mediated coupling of Fe and N cycles by nitrate-reducing Fe(II)-oxidizing bacteria in littoral freshwater sediments. *Appl Environ Microbiol* 2018;**84**:1–14. https://doi.org/10.1128/AEM.02013-17.
7. Huang J, Mellage A, Garcia JP *et al.* Metabolic performance and fate of electrons during nitrate-reducing Fe(II) oxidation by the autotrophic enrichment culture KS grown at different initial Fe/N ratios. *Appl Environ Microbiol* 2023;**89**:e0019623. https://doi.org/10.1128/aem.00196-23.

8. Chen D, Cheng K, Liu T *et al.* Novel insight into microbially mediated nitrate-reducing Fe(II) oxidation by *Acidovorax* sp. strain BoFeN1 using dual N-O isotope fractionation. *Environ Sci Technol* 2023;**57**:12546–55. Available from: https://doi.org/10.1021/acs.est.3c02329. https://pubmed.ncbi.nlm.nih.gov/37535944/.
9. Straub KL, Benz M, Schink B *et al.* Anaerobic, nitrate-dependent microbial oxidation of ferrous iron. *Appl Environ Microbiol* 1996;**62**:1458–60. https://doi.org/10.1128/aem.62.4.1458-1460.1996.
10. Bryce C, Blackwell N, Schmidt C *et al.* Microbial anaerobic Fe(II) oxidation – ecology„ mechanisms and environmental implications. *Environ Microbiol* 2018;**20**:3462–83. Available from: http://doi.wiley.com/10.1111/1462-2920.14328.
11. Huang YM, Jakus N, Straub D *et al.* '*Candidatus* ferrigenium straubiae' sp. nov., '*Candidatus* ferrigenium bremense' sp. nov., '*Candidatus* ferrigenium altingense' sp. nov., are autotrophic Fe(II)-oxidizing bacteria of the family *Gallionellaceae*. *Syst Appl Microbiol* 2022;**45**:126306. https://doi.org/10.1016/j.syapm.2022.126306.
12. Price A, Macey MC, Miot J *et al.* Draft genome sequences of the nitrate-dependent iron-oxidizing *Proteobacteria Acidovorax* sp. strain BoFeN1 and *Paracoccus pantotrophus* strain KS1. *Microbiol Resour Announc* 2018;**7**:1–2. https://doi.org/10.1128/MRA.01050-18.
13. Huang Y, Straub D, Blackwell N *et al.* Meta-omics reveal *Gallionellaceae* and *Rhodanobacter* species as interdependent key players for Fe(II) oxidation and nitrate reduction in the autotrophic enrichment culture KS. *Appl Environ Microbiol* 2021;**87**:e0049621. https://doi.org/10.1128/AEM.00496-21.
14. Weber KA, Achenbach LA, Coates JD. Microorganisms pumping iron: anaerobic microbial iron oxidation and reduction. *Nat Rev Microbiol* 2006;**4**:752–64. Available from: https://doi.org/10.1038/nrmicro1490. https://digitalcommons.unl.edu/bioscifacpub.
15. Hedrich S, Schlömann M, Barrie Johnson D. *The Iron-Oxidizing Proteobacteria [Internet]*. Vol. **157**, Great Britain: Microbiology. Microbiology Society; 2011. 1551–64. Available from: https://www.microbiologyresearch.org/content/journal/micro/10.1099/mic.0.045344-0.
16. Kleerebezem R, Van Loosdrecht MCM. Thermodynamic and kinetic characterization using process dynamics: acidophilic ferrous iron oxidation by *Leptospirillum ferrooxidans*. *Biotechnol Bioeng* 2008;**100**:49–60. https://doi.org/10.1002/bit.21745.
17. Agudelo-Vera C, Avvedimento S, Boxall J *et al.* Drinking water temperature around the globe: understanding, policies, challenges and opportunities. *Water (Switzerland)* 2020;**12**:1049. https://doi.org/10.3390/w12041049.
18. Bowers RM, Kyrpides NC *et al.* Minimum information about a single amplified genome (MISAG) and a metagenome-assembled genome (MIMAG) of bacteria and archaea. *Nat Biotechnol* 2017;**35**:725–31. https://doi.org/10.1038/nbt.3893.
19. Garber AI, Nealson KH, Okamoto A *et al.* FeGenie: a comprehensive tool for the identification of iron genes and iron gene neighborhoods in genome and metagenome assemblies. *Front Microbiol* 2020;**11**:37. Available from: https://doi.org/10.3389/fmicb.2020.00037. https://github.com/Arkadiy-Garber/FeGenie.
20. Kanehisa M, Sato Y, Morishima K. BlastKOALA and GhostKOALA: KEGG tools for functional characterization of genome and metagenome sequences. *J Mol Biol* 2016;**428**:726–31. https://doi.org/10.1016/j.jmb.2015.11.006.
21. Pinto AJ, Marcus DN, Ijaz UZ *et al.* Metagenomic evidence for the presence of comammoxnitrospira-like bacteria in a drinking water system. *mSphere* 2016;**1**:1–15.
22. Parks DH, Chuvochina M, Waite DW *et al.* A standardized bacterial taxonomy based on genome phylogeny substantially revises the tree of life. *Nat Biotechnol* 2018;**36**:996–1004. Available from: https://doi.org/10.1038/nbt.4229. https://www-nature-com.tudelft.idm.oclc.org/articles/nbt.4229.
23. Minh BQ, Schmidt HA, Chernomor O *et al.* IQ-TREE 2: new models and efficient methods for phylogenetic inference in the genomic era. *Mol Biol Evol* 2020;**37**:1530–4. Available from: https://doi.org/10.1093/molbev/msaa015. https://pubmed-ncbi-nlm-nih-gov.tudelft.idm.oclc.org/32011700/.
24. Anisimova M, Gascuel O. Approximate likelihood-ratio test for branches: a fast, accurate, and powerful alternative. *Syst Biol* 2006;**55**:539–52. Available from: https://doi.org/10.1080/10635150600755453. https://pubmed-ncbi-nlm-nih-gov.tudelft.idm.oclc.org/16785212/.
25. Schwertmann U, Cornell RM, Rao CNR, *et al. The Iron Oxides*. 2nd ed, Synthesis. Weinheim, Germany: Wiley-VCH GmbH & Co. KGaA, 2003, 694.
26. Lees H, Kwok SC, Suzuki I. The thermodynamics of iron oxidation by the ferrobacilli. *Can J Microbiol* 1968;**12**:6–8.
27. Müller V, Hess V. The minimum biological energy quantum. Vol. **8**, *Frontiers in Microbiology*. Switzerland: Frontiers Media S.A.; 2017. p. 2019.
28. Hayhurst AN, Lawrence AD. The reduction of the nitrogen oxides NO and N2O to molecular nitrogen in the presence of iron, its oxides, and carbon monoxide in a hot fluidized bed. *Combust Flame* 1997;**110**:351–65. https://doi.org/10.1016/S0010-2180(97)00085-0.
29. Costa E, Pérez J, Kreft JU. Why is metabolic labour divided in nitrification? *Trends Microbiol* 2006;**14**:213–9. https://doi.org/10.1016/j.tim.2006.03.006.
30. Pessi IS, Viitamäki S, Virkkala AM *et al.* In-depth characterization of denitrifier communities across different soil ecosystems in the tundra. *Environ Microbiomes* 2022;**17**:30–17. Available from: https://doi.org/10.1186/s40793-022-00424-2.
31. Huang Y-M, Straub D, Kappler A *et al.* A novel enrichment culture highlights core features of microbial networks contributing to autotrophic Fe(II) oxidation coupled to nitrate reduction. *Microb Physiol* 2021;**31**:280–95. Available from: https://doi.org/10.1159/000517083. https://www.karger.com/Article/FullText/517083.
32. Cheng B, Wang Y, Hua Y *et al.* The performance of nitrate-reducing Fe(II) oxidation processes under variable initial Fe/N ratios: the fate of nitrogen and iron species. *Front Environ Sci Eng* 2021;**15**:73. Available from: https://doi.org/10.1007/s11783-020-1366-2.
33. Jamieson J, Prommer H, Kaksonen AH *et al.* Identifying and quantifying the intermediate processes during nitrate-dependent iron(II). *Oxidation* 2018;**52**:5771–81. Available from: https://doi.org/10.1021/acs.est.8b01122. https://pubs.acs.org/sharingguidelines.
34. He S, Tominski C, Kappler A *et al.* Metagenomic analyses of the autotrophic Fe(II)-oxidizing, nitrate-reducing enrichment culture KS. *Appl Environ Microbiol* 2016;**82**:2656–68. https://doi.org/10.1128/AEM.03493-15.
35. Simon J, van Spanning RJM, Richardson DJ. The organisation of proton motive and non-proton motive redox loops in prokaryotic respiratory systems. *Biochim Biophys Acta Bioenerg* 2008;**1777**:1480–90. https://doi.org/10.1016/j.bbabio.2008.09.008.
36. Chen J, Strous M. Denitrification and aerobic respiration, hybrid electron transport chains and co-evolution. *Biochim Biophys Acta Bioenerg* 2013;**1827**:136–44. https://doi.org/10.1016/j.bbabio.2012.10.002.

37. Hu M, Chen P, Sun W *et al.* A novel organotrophic nitrate-reducing Fe(II)-oxidizing bacterium isolated from paddy soil and draft genome sequencing indicate its metabolic versatility. *RSC Adv* 2017;**7**:56611–20. https://doi.org/10.1039/C7RA09328D.
38. Jakus N, Blackwell N, Straub D *et al.* Presence of Fe(II) and nitrate shapes aquifer-originating communities leading to an autotrophic enrichment dominated by an Fe(II)-oxidizing Gallionellaceae sp. *FEMS Microbiol Ecol* 2021;**97**:1–14. Available from: https://doi.org/10.1093/femsec/fiab145. https://academic-oup-com.tudelft.idm.oclc.org/femsec/article/97/11/fiab145/6415198.
39. Gorski CA, Edwards R, Sander M *et al.* Thermodynamic characterization of iron oxide-aqueous Fe2+ redox couples. *Environ Sci Technol* 2016;**50**:8538–47. https://doi.org/10.1021/acs.est.6b02661.
40. Caltran I, Rietveld LC, Shorney-Darby HL *et al.* Separating NOM from salts in ion exchange brine with ceramic nanofiltration. *Water Res* 2020;**179**:115894. https://doi.org/10.1016/j.watres.2020.115894.
41. Van Cleemput O. Subsoils: chemo- and biological denitrification, N2O and N2 emissions. *Nutr Cycl Agroecosystems* 1998;**52**:187–94. Available from: https://link.springer.com/article/10.1023/A:1009728125678.
42. Tominski C, Heyer H, Lösekann-Behrens T *et al.* Growth and population dynamics of the anaerobic Fe(II)-oxidizing and nitrate-reducing enrichment culture KS. *Appl Environ Microbiol* 2018;**84**:2173–90. Available from: https://doi.org/10.1128/AEM.02173-17. http://aem.asm.org/.
43. Sorokin DY, Tikhonova TV, Koch H *et al.* Trichlorobacter ammonificans, a dedicated acetate-dependent ammonifier with a novel module for dissimilatory nitrate reduction to ammonia. *ISME J* 2023;**17**:1–10.https://doi.org/10.1038/s41396-023-01473-2.
44. Fredrickson JK, Zachara JM, Kennedy DW *et al.* Biogenic iron mineralization accompanying the dissimilatory reduction of hydrous ferric oxide by a groundwater bacterium. *Geochim Cosmochim Acta* 1998;**62**:3239–57. https://doi.org/10.1016/S0016-7037(98)00243-9.
45. Jolivet JP, Chanéac C, Tronc E. Iron oxide chemistry. From molecular clusters to extended solid networks. *Chem Commun* 2004;**4**:477–83. https://doi.org/10.1039/B304532N.
46. Vlek PLG, Blom TJM, Beek J *et al.* Determination of the solubility product of various iron hydroxides and Jarosite by the chelation method. *Soil Sci Soc Am J* 1974;**38**:429–32. https://doi.org/10.2136/sssaj1974.03615995003800030018x.
47. Bolger AM, Lohse M, Usadel B. Trimmomatic: a flexible trimmer for Illumina sequence data. *Bioinformatics* 2014;**30**:2114–20. Available from: https://pubmed.ncbi.nlm.nih.gov/24695404/.
48. Andrews S. FastQC: a quality control tool for high throughput sequence data [Online] [Internet]. 2010. Available from: http://www.bioinformatics.babraham.ac.uk/projects/fastqc/.
49. Sereika M, Kirkegaard RH, Karst SM *et al.* Oxford nanopore R10.4 long-read sequencing enables the generation of near-finished bacterial genomes from pure cultures and metagenomes without short-read or reference polishing. *Nat Methods* 2022;**19**:823–6. Available from: https://doi.org/10.1038/s41592-022-01539-7. https://www.nature.com/articles/s41592-022-01539-7.
50. Lin Y, Yuan J, Kolmogorov M *et al.* Assembly of long error-prone reads using de Bruijn graphs. *Proc Natl Acad Sci USA* 2016;**113**:E8396–405. Available from: https://doi.org/10.1073/pnas.1604560113.
51. Li H. Minimap2: pairwise alignment for nucleotide sequences. *Bioinformatics* 2018;**34**:3094–100. Available from: https://doi.org/10.1093/bioinformatics/bty191. https://academic.oup.com/bioinformatics/article/34/18/3094/4994778.
52. Vaser R, Sović I, Nagarajan N *et al.* Fast and accurate de novo genome assembly from long uncorrected reads. *Genome Res* 2017;**27**:737–46. Available from: https://doi.org/10.1101/gr.214270.116. https://genome.cshlp.org/content/27/5/737.full.
53. Vasimuddin M, Misra S, Li H *et al.* Efficient architecture-aware acceleration of BWA-MEM for multicore systems. In: *Proceedings - 2019 IEEE 33rd International Parallel and Distributed Processing Symposium, IPDPS 2019*, Rio de Janeiro, Brazil. Institute of Electrical and Electronics Engineers Inc., Washington, USA, 2019, 314–24.
54. Li H, Handsaker B, Wysoker A *et al.* The sequence alignment/map format and SAMtools. *Bioinformatics* 2009;**25**:2078–9. Available from: https://pubmed.ncbi.nlm.nih.gov/19505943/.
55. Kang DD, Li F, Kirton E, Thomas A, Egan R, An H, Wang Z MetaBAT 2: an adaptive binning algorithm for robust and efficient genome reconstruction from metagenome assemblies. *PeerJ [Internet]* 2019;**7**:e7359. Available from: https://doi.org/10.7717/peerj.7359.
56. Wu YW, Simmons BA, Singer SW. MaxBin 2.0: an automated binning algorithm to recover genomes from multiple metagenomic datasets. *Bioinformatics* 2016;**32**:605–7. Available from: https://doi.org/10.1093/bioinformatics/btv638. www.jbei.org.
57. Nissen JN, Johansen J, Allesøe RL *et al.* Improved metagenome binning and assembly using deep variational autoencoders. *Nat Biotechnol* 2021;**39**:555–60. https://doi.org/10.1038/s41587-020-00777-4.
58. CM KS, Probst AJ, Sharrar A *et al.* Recovery of genomes from metagenomes via a dereplication, aggregation and scoring strategy. *Nat Microbiol* 2018;**3**:836–43. Available from: https://doi.org/10.1038/s41564-018-0171-1. https://www.nature.com/articles/s41564-018-0171-1.
59. Parks DH, Imelfort M, Skennerton CT *et al.* CheckM: assessing the quality of microbial genomes recovered from isolates, single cells, and metagenomes. *Genome Res* 2015;**25**:1043–55. Available from: https://doi.org/10.1101/gr.186072.114. https://genome-cshlp-org.tudelft.idm.oclc.org/content/25/7/1043.full.
60. Parks DH, Chuvochina M, Chaumeil P-A *et al.* A complete domain-to-species taxonomy for bacteria and archaea. *Nat Biotechnol* 2020;**38**:1079–86. https://doi.org/10.1038/s41587-020-0501-8.
61. Arias-Carrasco R, Vásquez-Morán Y, Nakaya HI *et al.* StructRNAfinder: an automated pipeline and web server for RNA families prediction. *BMC Bioinformatics* 2018;**19**:1–7. Available from: https://bmcbioinformatics.biomedcentral.com/articles/10.1186/s12859-018-2052-2.
62. Chan PP, Lin BY, Mak AJ, Lowe TM. tRNAscan-SE 2.0: improved detection and functional classification of transfer RNA genes. *Nucleic Acids Res* 2021;**49**(16):9077–96. Available from: https://academic-oup-com.tudelft.idm.oclc.org/nar/article/49/16/9077/6355886. https://doi.org/10.1093/nar/gkab688.
63. Hyatt D, Chen GL, LoCascio PF *et al.* Prodigal: prokaryotic gene recognition and translation initiation site identification. *BMC Bioinformatics* 2010;**11**:1–11. Available from: https://bmcbioinformatics.biomedcentral.com/articles/10.1186/1471-2105-11-119.
64. Tatusova T, Dicuccio M, Badretdin A *et al.* NCBI prokaryotic genome annotation pipeline. *Nucleic Acids Res* 2016;**44**:6614–24. Available from: https://doi.org/10.1093/nar/gkw569. https://pubmed-ncbi-nlm-nih-gov.tudelft.idm.oclc.org/27342282/.

65. Altschul SF, Madden TL, Schäffer AA *et al.* Gapped BLAST and PSI-BLAST: a new generation of protein database search programs. *Nucleic Acids Res* 1997;**25**:3389–402. Available from: https://doi.org/10.1093/nar/25.17.3389. https://academic-oup-com.tudelft.idm.oclc.org/nar/article/25/17/3389/1061651.
66. Rost B. Twilight zone of protein sequence alignments. *Protein Eng Des Sel* 1999;**12**:85–94. Available from: https://doi.org/10.1093/protein/12.2.85. https://academic-oup-com.tudelft.idm.oclc.org/peds/article/12/2/85/1550637.
67. Kalyaanamoorthy S, Minh BQ, Wong TKF *et al.* ModelFinder: fast model selection for accurate phylogenetic estimates. *Nat Methods [Internet]* 2017;**14**:587–9. Available from: https://doi.org/10.1038/nmeth.4285. https://pubmed-ncbi-nlm-nih-gov.tudelft.idm.oclc.org/28481363/.
68. Thi Hoang D, Chernomor O, von Haeseler A *et al.* UFBoot2: improving the ultrafast bootstrap approximation. *Mol Biol Evol* 2017;**35**:518–22. Available from: https://doi.org/10.1093/molbev/msx281. http://www.iqtree.org.
69. Richter M, Rosselló-Móra R, Oliver Glöckner F *et al.* JSpeciesWS: a web server for prokaryotic species circumscription based on pairwise genome comparison. *Bioinformatics* 2016;**32**:929–31. Available from: https://doi.org/10.1093/bioinformatics/btv681. http://jspecies.ribohost.com/.